



ISTITUTO NAZIONALE DI RICERCA METROLOGICA
Repository Istituzionale

Skin effect in steel sheets under rotating induction

This is the author's accepted version of the contribution published as:

Original

Skin effect in steel sheets under rotating induction / Appino, Carlo; O., Hamrit; F., Fiorillo; C., Ragusa; O., de la Barrière; F., Mazaleyrat; M., Lobue. - In: INTERNATIONAL JOURNAL OF APPLIED ELECTROMAGNETICS AND MECHANICS. - ISSN 1383-5416. - 48:(2015), pp. 247-254. [10.3233/JAE-151995]

Availability:

This version is available at: 11696/31355 since: 2025-02-05T16:44:50Z

Publisher:

IOS

Published

DOI:10.3233/JAE-151995

Terms of use:

This article is made available under terms and conditions as specified in the corresponding bibliographic description in the repository

Publisher copyright

(Article begins on next page)

Skin effect in steel sheets under rotating induction

C. Appino¹, O. Hamrit², F. Fiorillo¹, C. Ragusa³, O. de la Barrière^{2a}, F. Mazaleyrat², M. LoBue²

¹Istituto Nazionale di Ricerca Metrologica (INRIM), Strada delle cacce 91, 10135 Torino, Italy

²SATIE, ENS Cachan, CNRS, UniverSud, 61 av. du Président Wilson, F-94230 Cachan, France

³Dipartimento Energia, Politecnico di Torino, C.so Duca degli Abruzzi 24, 10129 Torino, Italy

^a Corresponding author. Electronic address: barriere@satie.ens-cachan.fr, telephone: 0033147402125.

Abstract

By means of a newly developed broadband measuring setup we have overcome the usual upper limit for the test frequency, around a few hundred Hz, which is encountered in the two-dimensional characterization of magnetic steel sheets at technical inductions and we have measured the rotational losses in low-carbon steels up to 1 kHz and peak induction 1.7 T. An important piece of information is thus retrieved upon a frequency range useful to predict the performance of high-speed electrical machines. Our experiments, performed on thick (0.640 mm) laminations, have brought to light the emergence of the skin effect under rotational fields. This is revealed by an abrupt deviation of the excess loss component, calculated under the conventional loss separation procedure, from its well-known linear dependence on the square root of the frequency. A simple magnetic constitutive law under rotating induction is proposed and introduced into the electromagnetic diffusion equation, which is solved by finite elements coupled to a non-linear algorithm. The classical rotational eddy current loss, largely prevalent with respect to the hysteresis and excess loss components on approaching the kHz frequencies in low-carbon steels, is then calculated in the presence of skin effect, permitting one to achieve full analysis of the rotational losses and good predicting capability upon a broad range of frequencies and peak inductions.

16 1- Introduction

17 In electrical traction applications, compact geometry and maximum torque density of motors are obtained by
18 increasing the rotating speed [1, 2], with ensuing high conversion frequencies, greater iron losses, and decreasing
19 efficiency. A compromise must then be found at the design stage between these competing issues, a reason for
20 requiring accurate broadband magnetic loss characterization of the laminations used in the machine cores and a
21 relatively simple implementation of loss modeling. The loss decomposition procedure, including the case of
22 distorted induction, is the standard modeling response to the loss phenomenology at low-to-medium frequencies,
23 where the skin effect can be neglected [3, 4]. Starting from solid physical analysis, it provides a simple three-
24 term expression for the measured energy loss $W(f) = W_{\text{hyst}} + W_{\text{class}}(f) + W_{\text{exc}}(f)$, where the quasi-static term W_{hyst}
25 combines with a dynamic contribution $W_{\text{dyn}}(f) = W_{\text{class}}(f) + W_{\text{exc}}(f)$, the sum of the classical and the excess
26 components, which depend on the magnetizing frequency like f and $f^{1/2}$, respectively [3]. When, under
27 increasing f , eddy current shielding gives rise to skin depth comparable to or lower than the lamination half-
28 thickness, straightforward loss separation cannot be accomplished and the calculation of the dynamic loss
29 component via the electromagnetic diffusion equation requires modeling (for example, via the Preisach model of
30 hysteresis) of the constitutive equation of the material and the use of numerical methods [5-8].

31 It has been shown that conventional loss separation can be applied, in the absence of skin effect, to the two-
32 dimensional losses, and one can express, in particular, the rotational losses as $W^{(\text{ROT})}(f) = W_{\text{hyst}}^{(\text{ROT})} + W_{\text{class}}^{(\text{ROT})}(f)$
33 $+ W_{\text{exc}}^{(\text{ROT})}(f)$, with the same $W_{\text{class}}^{(\text{ROT})} \propto f$ and $W_{\text{exc}}^{(\text{ROT})} \propto f^{1/2}$ dependences found under alternating fields [9]. Very
34 little is known, however, on the behavior of the rotational losses beyond a few hundred Hz [10], that is, under the
35 regimes pertaining to high-speed electrical machines, where skin effect will expectedly take place.

36 We have employed a recently developed 2D setup, based on a three-phase magnetizer [11], to attain
37 rotational induction levels of technical interest (e.g. $J_p = 1.5$ T and beyond) in non-oriented steel sheets up to the
38 kHz range [12]. We have investigated, in particular, the rotational loss behavior versus frequency of low-carbon
39 steel sheets, 0.640 mm thick, up to 1 kHz and peak polarization $J_p = 1.7$ T. Conductivity and thickness of these
40 sheets are sufficient to generate a surge of the skin effect already at power frequencies. A sort of frequency
41 threshold for it is in fact identified, where an attendant sharp deviation of $W_{\text{exc}}^{(\text{ROT})}$ from the usual $f^{1/2}$ dependence
42 is put in evidence when applying the standard loss decomposition procedure. This appears to be a unique simple
43 experimental route to direct recognition of growing skin effect. It also highlights the conceptually important role
44 of the excess component in the loss analysis, even if, as in the present case, it marginal contributes to the total
45 loss figure. To calculate the classical loss, by far the largest component in the upper frequency range, it is
46 recognized that, thanks to the near-isotropic properties of the material, the magnetic constitutive law $B(H)$ under
47 rotational field can be well approximated, along any of two orthogonal directions, by a simple relationship
48 between complex quantities of the type $\underline{B} = \underline{\mu}(\underline{H}) \cdot \underline{H}$. This permits one to solve the electromagnetic diffusion
49 equation by conventional numerical technique and to calculate $W_{\text{class}}^{(\text{ROT})}(f)$, eventually attaining good prediction
50 of $W^{(\text{ROT})}(f)$ upon the whole investigated frequency range.

51

52 2. Experimental results: evidence for the skin effect

53 A three-phase magnetizer, especially designed to reach high frequencies [11], has been employed in the
 54 measurement of the magnetic losses in low-carbon steel sheets (density $\delta = 7850 \text{ kg/m}^3$, thickness $d = 0.640 \text{ mm}$,
 55 resistivity $\rho = 12.51 \cdot 10^{-8} \text{ } \Omega \cdot \text{m}$) under digitally controlled circular flux loci [13]. The magnetic losses have been
 56 measured by the fieldmetric method [14-15] on 80 mm diameter circular samples, accurately centred in the
 57 stator-like magnetizer. A small air-gap of 1 mm permits one to minimize the required exciting power, which is
 58 supplied by triple DC-20 kHz 5 kVA power amplifier (CROWN 5000VZ). The orthogonal B and H windings are
 59 placed on a 20 mm \times 20 mm measuring area at the centre of the disk. The measurements are repeated, for any
 60 polarization and frequency value, under clockwise and counterclockwise rotation and their average is taken as
 61 the resulting loss figure $W^{(\text{ROT})}(J_p, f)$. Fig. 1 shows the experimental dependence of the measured rotational loss
 62 on J_p (negligibly different everywhere from the peak induction B_p) up to 1.7 T for frequencies ranging between 2
 63 Hz and 1kHz. It is noted how the maximum of $W^{(\text{ROT})}(f)$ versus J_p , occurring around $J_p = 1.5 \text{ T}$, tends to
 64 disappear beyond about 50 Hz, because of the growing influence of the monotonically increasing classical loss
 65 component. It is also remarked that the upper values of the here attained product $J_p \cdot f$ (e.g., $J_p = 1.5 \text{ T}$ at $f = 1$
 66 kHz) are significantly larger than present literature limits [10].

67 According to the standard analysis performed at power frequencies in nonoriented Fe-Si laminations [9], the
 68 rotational hysteresis $W_{\text{hyst}}^{(\text{ROT})}$ is found by extrapolating $W^{(\text{ROT})}(J_p, f)$ to $f = 0$ and we calculate the classical loss
 69 $W_{\text{class}}^{(\text{ROT})}(f)$ as

$$70 \quad W_{\text{class}}^{(\text{ROT})}(B_p, f) = \frac{\pi^2}{3} \cdot \frac{d^2 B_p^2}{\rho} f. \quad [\text{J/m}^3] \quad (1)$$

71 By making the difference $W_{\text{diff}}^{(\text{ROT})}(f) = W^{(\text{ROT})}(f) - W_{\text{class}}^{(\text{ROT})}(f) = W_{\text{hyst}}^{(\text{ROT})} + W_{\text{exc}}^{(\text{ROT})}(f)$, we obtain the behaviors
 72 shown in Fig. 2a (symbols), where the quantity $W_{\text{diff}}^{(\text{ROT})}(f)$ is plotted against $f^{1/2}$ for three different induction
 73 levels. $W_{\text{diff}}^{(\text{ROT})}(f)$ strongly deviates, beyond a threshold frequency value f_{thr} , from the usual $f^{1/2}$ dependence (the
 74 straight lines in Fig. 2a) experimentally observed below and around power frequencies in 3 wt% Fe-Si
 75 laminations [16]. $W_{\text{diff}}^{(\text{ROT})}(f)$ follows opposite outward trends with respect to the $f^{1/2}$ straight line below and above
 76 $J_p \sim 1 \text{ T}$, because $W_{\text{class}}^{(\text{ROT})}(f)$ tends either to lower or faster than linear dependence on f and Eq. (1) no more
 77 applies. Such behavior of $W_{\text{class}}^{(\text{ROT})}(f)$ replicates the phenomenology of the alternating classical loss in the
 78 presence of the skin effect [3-5] and is further put in evidence by the statistical analysis of the magnetic objects
 79 (MO), as defined in Bertotti's theory [3]. Fig. 2 shows the dramatic departure of the number $n(H_{\text{exc}})$ of active
 80 MOs from the linear increase with $H_{\text{exc}} = W_{\text{exc}}^{(\text{ROT})}/4J_p$ predicted using Eq. (1). The sharp turnaround of $n(H_{\text{exc}})$
 81 occurs exactly at the frequency f_{thr} . The statistical loss analysis provides then us with a direct and unique method
 82 to detect the surge of the skin effect in magnetic sheets, even though, like in the present case, $W_{\text{exc}}^{(\text{ROT})}$
 83 contributes by a small proportion to $W^{(\text{ROT})}$. We have for example, at $J_p = 1.2 \text{ T}$ and $f_{\text{thr}} = 100 \text{ Hz}$, the total
 84 rotational loss $W^{(\text{ROT})} = 360.5 \text{ mJ/kg}$, composed of $W_{\text{hyst}}^{(\text{ROT})} = 139.5 \text{ mJ/kg}$, $W_{\text{class}}^{(\text{ROT})} = 197.5 \text{ mJ/kg}$, and $W_{\text{exc}}^{(\text{ROT})}$
 85 $= 23.5 \text{ mJ/kg}$. It is remarked that, given the mechanism of the magnetization rotation in nonoriented materials,
 86 there is no room for classical loss formulations deriving from the saturation wave model, as sometimes proposed

87 in the literature [17].

88 Having thus experimentally identified a threshold frequency for the skin effect, we essentially need to
89 proceed towards a novel formulation for $W_{\text{class}}^{(\text{ROT})}(f)$, by which we can cover the rotational loss properties upon
90 the whole broad frequency range.

92 3. Skin effect and classical eddy current losses under circular induction

93 3.1 A simplified constitutive equation

94 Let us take the sheet sample midplane as the xy -plane and assume the coordinate $z = 0$ at the center of the
95 disk sample. The magnetization vector is assumed to rotate at constant angular velocity $\omega = 2\pi f$. We need to
96 define a constitutive equation for the material under rotating field, paralleling the usual case of alternating field,
97 where such equation coincides with the static hysteresis loop and a hysteresis model must be worked out [4, 18].
98 Remarkably, a simple magnetic constitutive law can be adopted with circular polarization in nonoriented alloys,
99 under the following assumptions: 1) The constitutive relationship is rate independent. This amounts to assume,
100 according to the experiments, that in the range of frequencies of interest (i.e., beyond f_{thr}) the excess loss figure
101 $W_{\text{exc}}^{(\text{ROT})}$ is much smaller than $W_{\text{hyst}}^{(\text{ROT})}$ and $W_{\text{class}}^{(\text{ROT})}$; 2) The material anisotropy can be neglected. We
102 approximate here this condition by substituting, at each frequency, the experimental magnetic field locus $\mathbf{H}(f)$
103 associated with the circular \mathbf{B} -locus (of modulus $B_p = |\mathbf{B}|$) with an equivalent circular \mathbf{H} -locus of same area and
104 radius $H(f) = |\mathbf{H}(f)|$, emulating the condition of a perfectly isotropic material. By extrapolating this procedure to f
105 $= 0$, the limiting circle of radius $H_0 = |\mathbf{H}_0|$ is obtained, with \mathbf{B} lagging behind \mathbf{H}_0 by the angle θ_{hyst} . Under the
106 isotropic approximation, the sinusoidal \mathbf{H} and \mathbf{B} components are identical along the x and y axes and the energy
107 loss

$$108 \quad W^{(\text{ROT})}(B_p, f) = \oint \mathbf{H} \cdot d\mathbf{B} = \int_0^{1/f} (H_x \cdot dB_x / dt + H_y \cdot dB_y / dt) = W_x + W_y = 2W_x, \quad [\text{J/m}^3] \quad (2)$$

109 can be written in the quasi-static limit as $W_{\text{hyst}}^{(\text{ROT})} = 2\pi H_0 B_p \omega \sin(\theta_{\text{hyst}})$. The phase shift is then obtained as

$$110 \quad \theta_{\text{hyst}}(H_0) = \arcsin \left[\frac{W_{\text{hyst}}^{(\text{ROT})}(B_p)}{2\pi H_0 B_p} \right]. \quad (3)$$

111 At the same time, the complex permeability, embodying the constitutive equation for the material under
112 rotational field, is given by

$$113 \quad \underline{\mu}(H_0) = \mu(H_0) \exp[-i\theta_{\text{hyst}}(H_0)] \quad (4)$$

114 (with $i^2 = -1$), where $\mu(H_0) = B_p/H_0$. Both $\underline{\mu}(H_0)$ and θ_{hyst} are time-independent and evolve with the polarization
115 level in the investigated material as shown in Fig. 4. The complex constitutive equations for the x and y
116 directions can thus be expressed as $\underline{B}_x = \underline{\mu}(H_x)\underline{H}_x$ and $\underline{B}_y = \underline{\mu}(H_y)\underline{H}_y$, with $H_x = |\underline{H}_x|$ and $H_y = |\underline{H}_y|$.

117 3.2 Diffusion equation and classical loss

118 The electromagnetic diffusion equation, controlling the magnetic field penetration in the sheet, is written,
119 under the usual assumption of infinitely extended xy -plane,

$$120 \quad \frac{\partial^2 \underline{H}_x(z)}{\partial z^2} = i\omega\sigma \underline{B}_x(z) \quad \frac{\partial^2 \underline{H}_y(z)}{\partial z^2} = i\omega\sigma \underline{B}_y(z) \quad (5)$$

121 where all the local quantities depend only on z . Introducing the constitutive equations in Eq. (5) we get

$$122 \quad \frac{\partial^2 \underline{H}_x(z)}{\partial z^2} = i\omega\sigma \underline{\mu}(H_x) \underline{H}_x \quad \frac{\partial^2 \underline{H}_y(z)}{\partial z^2} = i\omega\sigma \underline{\mu}(H_y) \underline{H}_y, \quad (6)$$

123 to be solved under the boundary conditions

$$124 \quad \left. \frac{\partial \underline{H}_x(z)}{\partial z} \right|_{z=0} = 0 \quad \left. \frac{\partial \underline{H}_y(z)}{\partial z} \right|_{z=0} = 0 \quad (7)$$

125

$$126 \quad \left. \frac{\partial \underline{H}_x(z)}{\partial z} \right|_{z=d/2} = i\omega\sigma \frac{d}{2} B_p \quad \left. \frac{\partial \underline{H}_y(z)}{\partial z} \right|_{z=d/2} = i\omega\sigma \frac{d}{2} B_p, \quad (8)$$

127 imposed by the symmetry of the magnetic field profile with respect to the $z=0$ plane (Neumann condition) and
 128 the requirement of a mean circular induction B_p across the sample thickness, respectively. This problem is non
 129 linear, because $\underline{\mu}$ depends on $|\underline{H}|$. We thus discretize Eq. (5) versus z by the Finite Elements Method and we
 130 apply the Fixed Point (FP) iterative technique [5] to solve the non linearity. Its solution provides the $\underline{H}(z)$ profile,
 131 by which we can compute, via the constitutive equation, the classical loss $W_{\text{class}}^{(\text{ROT}, \text{FP})}$ and obtain the hysteresis
 132 loss component $W_{\text{hyst}}^{(\text{ROT})}$. Since the induction profile through the sample cross-section evolves with f , the same
 133 holds for $W_{\text{hyst}}^{(\text{ROT})}$, as shown in Fig. 5. This behavior replicates to some extent the skin effect related increase of
 134 the hysteresis loss with f observed under alternating fields [5, 7], but for the decrease of $W_{\text{hyst}}^{(\text{ROT})}$ at the highest J_p
 135 values. Such a decrease is consistent with the experimental dependence of $W_{\text{hyst}}^{(\text{ROT})}$ on J_p . After having attained a
 136 maximum value, it tends to zero on approaching the saturation, following the disappearance of the domain walls.
 137 If we define the quantity $W^{(\text{ROT}, \text{FP})} = W_{\text{hyst}}^{(\text{ROT})} + W_{\text{class}}^{(\text{ROT}, \text{FP})}$, the sum of the so-calculated hysteresis and classical
 138 losses, we find that it accounts for most of the measured loss $W_{\text{exp}}^{(\text{ROT})}$ beyond f_{thr} , while the conventional loss
 139 separation holds below this threshold. Comparison of $W_{\text{exp}}^{(\text{ROT})}$ with $W^{(\text{ROT}, \text{FP})}$ is provided in Fig. 6 at $f = 1$ kHz
 140 and $f = 100$ Hz. In both cases the excess loss, though crucial to the identification of the threshold frequency f_{thr}
 141 via Eq. (1), turns out to be a few percent of the total loss only. It is observed how $W_{\text{class}}^{(\text{ROT})}$, calculated with Eq.
 142 (1), overestimates the measured loss at $f = 1$ kHz and low inductions, while falling short of $W_{\text{class}}^{(\text{ROT}, \text{FP})}$ at high
 143 inductions, consistent with the results reported in Fig. 2.

144 We might inquire about a possible approximate expression for the classical rotational loss with skin effect
 145 where, as often done with the alternating regime [3, 19], a linear material is considered. With constant complex
 146 permeability $\underline{\mu}$, uniform across the lamination depth and depending only on the mean value B_p , we obtain a linear
 147 diffusion equation, which can be analytically solved. If the correspondingly calculated classical loss is
 148 $W_{\text{class}}^{(\text{ROT}, \text{LIN})}$, a ratio $F_{\text{class}}^{(\text{LIN})} = W_{\text{class}}^{(\text{ROT}, \text{LIN})} / W_{\text{class}}^{(\text{ROT})}$ is obtained through the equation

149

150

$$F_{\text{class}}^{(\text{LIN})}(d/\delta) = 3 \frac{(\sinh a_+ / a_+ - \sinh a_- / a_-)}{\cosh a_+ - \cos a_-} \quad (9)$$

151

152

153

154

155

156

157

158

159

where $\delta = 1/(\pi|\underline{\mu}|\sigma)^{1/2}$ is the skin depth and $a_{\pm} = (1 \pm \delta) d/\delta$, with $\delta = \tan(0.5\delta \arg(\underline{\mu}))$, is a dimensionless quantity. It is interesting to parallel the ratio $F_{\text{class}}^{(\text{LIN})}$ with the one concerning the previous numerical solution for the classical loss $F_{\text{class}}^{(\text{FP})} = W_{\text{class}}^{(\text{ROT,FP})}/W_{\text{class}}^{(\text{ROT})}$. These ratios are shown as a function of d/δ , with the frequency ranging between DC and 1 kHz, for different values of J_p . The linear model, always providing a ratio $F_{\text{class}}^{(\text{LIN})} < 1$, cannot account for the effect of saturation on the lamination edges, a feature that can properly dealt with only by $W_{\text{class}}^{(\text{ROT,FP})}$. Remarkably, at high inductions, where $F_{\text{class}}^{(\text{FP})} \geq 1$ (but relatively close to 1, as shown in Fig. 7), assuming $F_{\text{class}} = 1$ (i.e. neglecting the skin effect) provides a better approximation of the experiments than the linear model.

159

4. Conclusions

160

161

162

163

164

165

166

167

168

169

170

Magnetic losses have been measured under circular induction in 0.640 mm tick low-carbon steel laminations up to frequencies of 1 kHz and peak polarization level $J_p = 1.7$ T. Relevant skin effect takes place, depending on the J_p value, starting from a few ten Hz, as uniquely revealed by the loss decomposition procedure, performed according to the statistical theory of losses. It is demonstrated that the classical loss component, always dominant beyond the threshold frequency for the skin effect, can be accurately computed exploiting a simplified magnetic constitutive law of the material under rotational field. It is also shown that the extreme simplification of assuming a fully linear approximation for the diffusion equation can provide acceptable results only at low induction levels.

- 172 [1] K.M. Rahman and S.E. Sculz, Design of high-efficiency and high-torque-density switched reluctance motor
173 for vehicle propulsion, *IEEE Trans. Ind. Appl.*, **38** (2002), 1500-1507.
- 174 [2] S. Niu, . Ho, W. Fu, and J. Zhu, Eddy current reduction in High-Speed Machines and Eddy Current Loss
175 Analysis With Multislice Time-Stepping Finite-Element Method, *IEEE Trans. Magn.*, **48** (2012), 1007-
176 1010.
- 177 [3] G. Bertotti, *Hysteresis in Magnetism*, Academic Press, New York, 1998, Chap. 12.
- 178 [4] E. Barbisio, F. Fiorillo, and C. Ragusa, Predicting Loss in Magnetic Steels Under Arbitrary Induction
179 Waveform and With Minor Hysteresis Loops, *IEEE Trans. Magn.*, **40** (2004), 1810-1819.
- 180 [5] C. Appino, G. Bertotti, O. Bottauscio, F. Fiorillo, P. Tiberto, D. Binesti, J.P. Ducreux, M. Chiampi, and M.
181 Repetto, Power losses in thick steel laminations with hysteresis, *J. Appl. Phys.* **79** (1996), 4575-4577.
- 182 [6] V. Basso, G. Bertotti, O. Bottauscio, F. Fiorillo, M. Pasquale, M. Chiampi, and M. Repetto, Power losses in
183 magnetic laminations with hysteresis: finite element modeling and experimental validation, *J. Appl. Phys.*
184 **81** (1997), 5606-5608.
- 185 [7] S. E. Zirka, Y.I. Moroz, P. Marketos, and A.J. Moses, Evolution of power loss components with induction
186 level and frequency, *J. Magn. Magn. Mater.* **320** (2008), e1039-e1043.
- 187 [8] C. Beatrice, C. Appino, O. de la Barrière, F. Fiorillo, and C. Ragusa, Broadband magnetic losses in Fe-Si
188 and Fe-Co laminations, *IEEE Trans. Magn.*, **50** (2014), 6300504.
- 189 [9] C. Appino, C. Ragusa, and F. Fiorillo, Can rotational magnetization be theoretically assessed?, *Int. J. Appl.*
190 *Electromagn. Mech.*, **44** (2014), 355-370.
- 191 [10] Y. Li, J. G. Zhu, Q. Yang, Z. W. Lin, Y. Guo, and C. Zhang, Study on rotational hysteresis and core loss
192 under three dimensional magnetization, *IEEE Trans. Magn.*, **47** (2011), 3520-3523.
- 193 [11] O. de la Barrière, C. Appino, F. Fiorillo, C. Ragusa, M. Lecrivain, L. Rocchino, H. Ben Ahmed, M. Gabsi,
194 F. Mazaleyrat, and M. LoBue, Extended frequency analysis of magnetic losses under rotating induction in
195 soft magnetic composites, *J. Appl. Phys.*, **111** (2012), 07E325.
- 196 [12] C. Appino, O. de la Barrière, C. Beatrice, F. Fiorillo, and C. Ragusa, Rotational magnetic losses in
197 nonoriented Fe-Si and Fe-Co laminations up to the kilohertz range, *IEEE Trans. Magn.*, **50** (2014), to
198 appear.
- 199 [13] C. Ragusa and F. Fiorillo, A three-phase single sheet tester with digital control of flux loci based on the
200 contraction mapping principle, *J. Magn. Magn. Mater.*, vol. 304, no. 2 (2006), pp. e568-e570.
- 201 [14] Y. Guo, J. Zhu, J. Zhong, H. Lu, and J. Jin, Measurement and modeling of rotational core losses of soft
202 magnetic materials used in electrical machines: a review, *IEEE Trans. Magn.*, **44** (2008), 279-291.
- 203 [15] E. Cardelli, A. Faba, and F. Tissi, *Int. J. Appl. Electromagn. Mech.*, **44** (2014), 331-338.
- 204 [16] C. Appino, F. Fiorillo, and C. Ragusa, One-dimensional/two-dimensional loss measurements up to high
205 inductions, *J. Appl. Phys.* **105** (2009), 07E718.
- 206 [17] S. Steentjes, S.E. Zirka, Y.E. Moroz, E.Y. Moroz, and K. Hameyer, Dynamic magnetization model of
207 nonoriented steel sheets, *IEEE Trans. Magn.*, **50** (2014), 7300204.
- 208 [18] S.E. Zirka, Y.I. Moroz, P. Marketos, and A.J. Moses, Viscosity-based magnetodynamic model of soft
209 magnetic materials, *IEEE Trans. Magn.*, **42** (2006), 2121-2132.
- 210 [19] I.D. Mayergoyz, F.M. Abdel-Kader, F.P. Emad, On penetration of electromagnetic fields into nonlinear
211 conducting ferromagnetic media, *J. Appl. Phys.*, **55** (1984), 618-628.
- 212

213
 214
 215
 216
 217
 218
 219
 220
 221
 222
 223
 224
 225
 226
 227
 228
 229
 230
 231
 232
 233
 234
 235
 236
 237
 238
 239
 240
 241
 242
 243
 244
 245
 246
 247
 248
 249
 250
 251
 252
 253
 254
 255
 256

Figure captions

Fig. 1 – Rotational energy loss vs. J_p measured in a 0.640 mm thick low-carbon steel sheet in the range of frequencies 2 Hz - 1 kHz.

Fig. 2 – a) The experimental values of $W_{\text{diff}}^{(\text{ROT})}(f) = W^{(\text{ROT})}(f) - W_{\text{class}}^{(\text{ROT})}(f)$ (symbols), with $W_{\text{class}}^{(\text{ROT})}(f)$ given by Eq. (1), diverge from the standard $f^{1/2}$ law beyond a threshold frequency, signaling the surge of the skin effect. b) At the same frequency the correspondingly calculated number of active magnetic objects $n(H_{\text{exc}})$ versus H_{exc} behavior suffers a sharp turnabout.

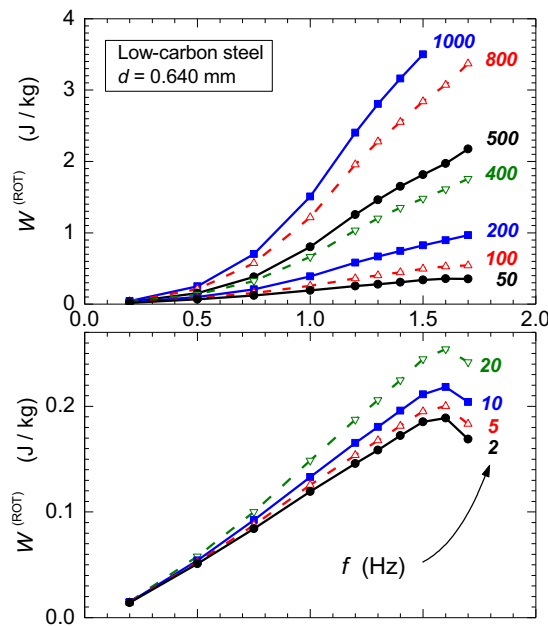
Fig. 3 – The experimental quasi-static H -locus is assimilated to a circular locus of same area, belonging to the equivalent perfectly isotropic material.

Fig. 4 – Quasi-static rotational permeability $|\underline{\mu}| = B_p / H_0$ and related angular delay \square_{hyst} of B_p versus the rotating field H_0

Fig. 5 – Skin effect dependent evolution of the hysteresis energy loss with frequency. Decrease of $W_{\text{hyst}}^{(\text{ROT})}$ with f is observed at highest J_p values, because the material attains saturation on the outer sheet layers.

Fig. 6 – Measured rotational loss $W_{\text{exp}}^{(\text{ROT})}$ versus polarization J_p at $f=1$ kHz and $f=100$ Hz and its comparison with the quantity $W^{(\text{ROT,FP})} = W_{\text{hyst}}^{(\text{ROT})} + W_{\text{class}}^{(\text{ROT,FP})}$ (solid line) calculated via the electromagnetic diffusion equation and its solution by the Fixed Point technique. The dash-dotted lined shows the behavior of $W_{\text{class}}^{(\text{ROT})}$ calculated with the standard Eq. (1).

Fig. 7 - Ratios $F_{\text{class}}^{(\text{FP})} = W_{\text{class}}^{(\text{ROT,FP})} / W_{\text{class}}^{(\text{ROT})}$ and $F_{\text{class}}^{(\text{LIN})} = W_{\text{class}}^{(\text{ROT,LIN})} / W_{\text{class}}^{(\text{ROT})}$ (with $W_{\text{class}}^{(\text{ROT})}$ given by Eq. (1)) calculated by the numerical method with Fixed Point iteration and the linear method. d / δ is the ratio between the sheet thickness and the skin depth.



257

258

259

260

261

262

263

Fig. 1 – Rotational energy loss versus circular polarization J_p measured in a 0.640 mm thick low-carbon steel sheet in the frequency range 2 Hz - 1 kHz.

264
 265
 266
 267
 268
 269
 270
 271
 272
 273
 274
 275
 276
 277
 278
 279
 280
 281
 282
 283
 284
 285
 286
 287
 288
 289
 290
 291
 292
 293
 294
 295
 296
 297
 298

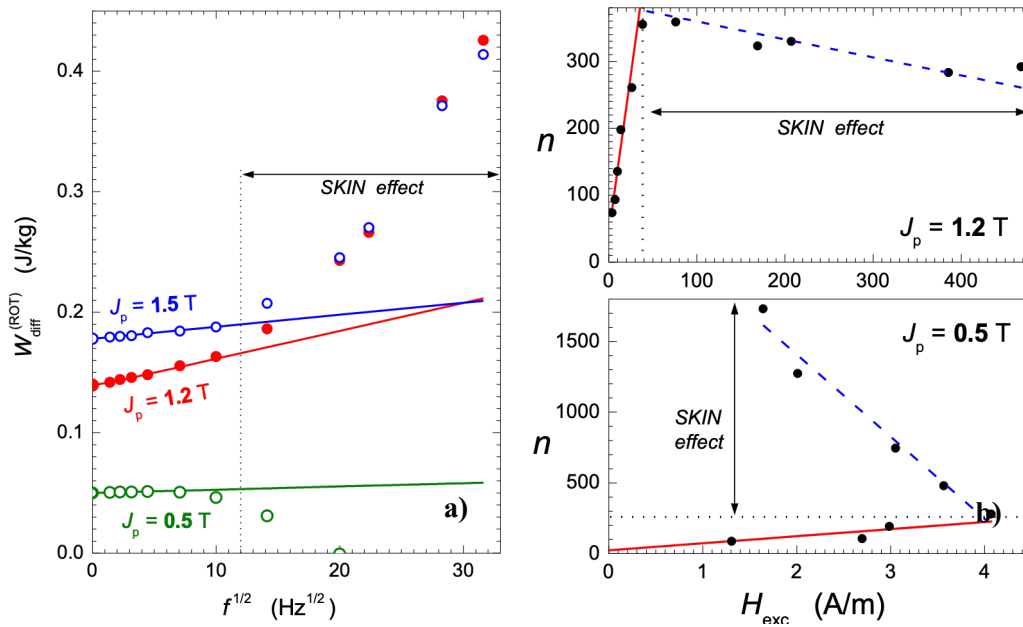
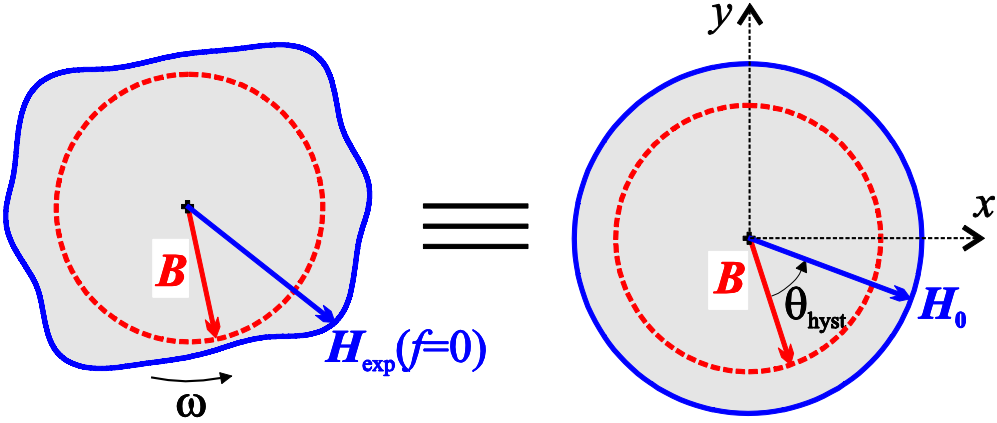


Fig. 2 – a) The experimental values of $W_{\text{diff}}^{(\text{ROT})}(f) = W^{(\text{ROT})}(f) - W_{\text{class}}^{(\text{ROT})}(f)$ (symbols), with $W_{\text{class}}^{(\text{ROT})}(f)$ given by Eq. (1), diverge from the standard $f^{1/2}$ law beyond a threshold frequency, signaling the surge of the skin effect. b) At the same frequency the correspondingly calculated number of active magnetic objects $n(H_{\text{exc}})$ versus H_{exc} behavior suffers a sharp turnabout.

299
300
301
302
303
304
305
306

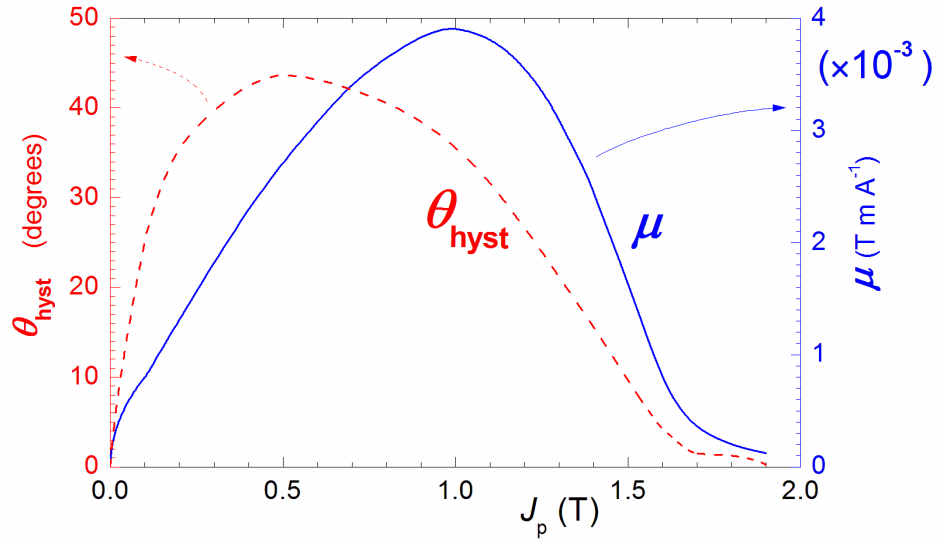


307
308
309

Fig. 1

Fig. 3 – The experimental quasi-static H -locus is assimilated to a circular locus of same area, belonging to the equivalent perfectly isotropic material.

310
311
312
313
314
315
316
317
318



319
320
321
322
323
324
325
326
327
328
329
330
331
332
333
334
335
336
337
338
339
340

Fig. 4 – Quasi-static rotational permeability $|\underline{\mu}| = B_p / H_0$ and related angular delay θ_{hyst} of B_p versus the rotating field H_0

341
342
343
344
345
346
347
348
349
350
351
352
353
354
355
356
357
358
359
360
361
362
363
364
365
366
367
368
369
370
371
372
373
374
375
376
377
378
379
380
381
382
383
384
385
386
387
388
389

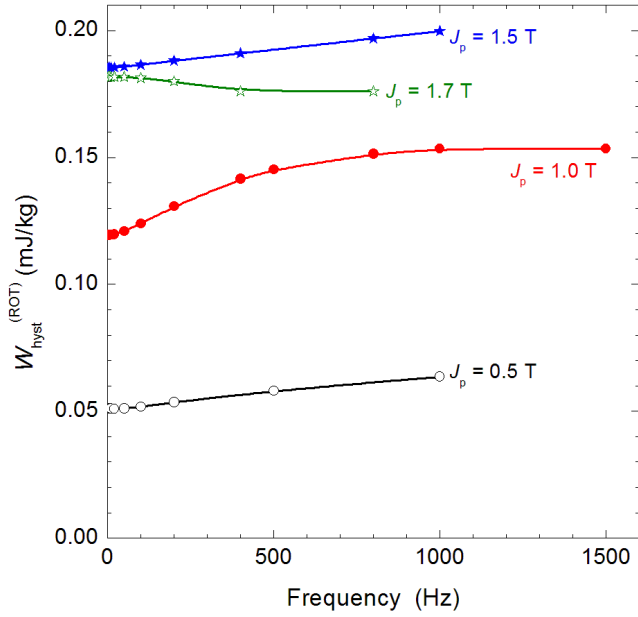


Fig. 5 – Skin effect dependent evolution of the hysteresis energy loss with frequency. Decrease of $W_{\text{hyst}}^{(\text{ROT})}$ with f is observed at highest J_p values, because the material attains saturation in the outer sheet layers.

390
 391
 392
 393
 394
 395
 396
 397
 398
 399
 400
 401
 402
 403
 404
 405
 406
 407
 408
 409
 410
 411
 412
 413
 414
 415
 416
 417
 418
 419
 420
 421
 422
 423
 424
 425
 426
 427
 428
 429
 430
 431
 432
 433
 434
 435
 436
 437
 438
 439

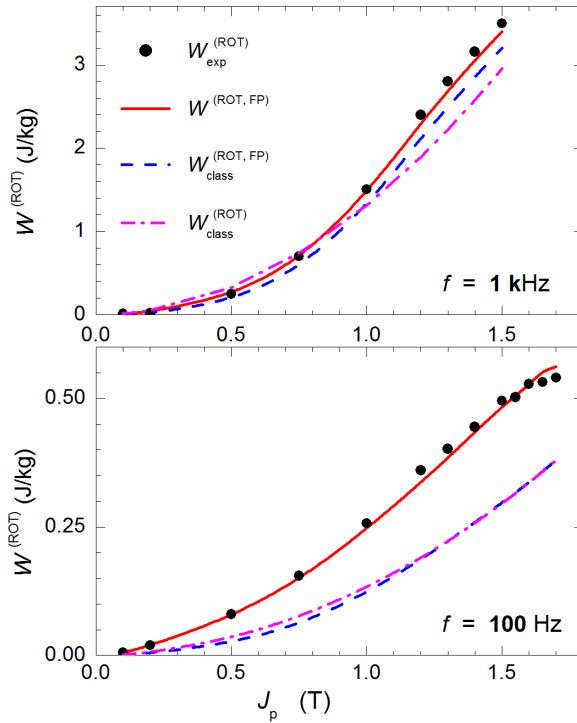


Fig. 6 – Measured rotational loss $W_{exp}^{(ROT)}$ versus polarization J_p at $f = 1 \text{ kHz}$ and $f = 100 \text{ Hz}$ and its comparison with the quantity $W^{(ROT, FP)} = W_{hyst}^{(ROT)} + W_{class}^{(ROT, FP)}$ (solid line) calculated via the electromagnetic diffusion equation and its solution by the Fixed Point technique. The dash-dotted lined shows the behavior of $W_{class}^{(ROT)}$ calculated with the standard Eq. (1).

440
 441
 442
 443
 444
 445
 446
 447
 448
 449
 450

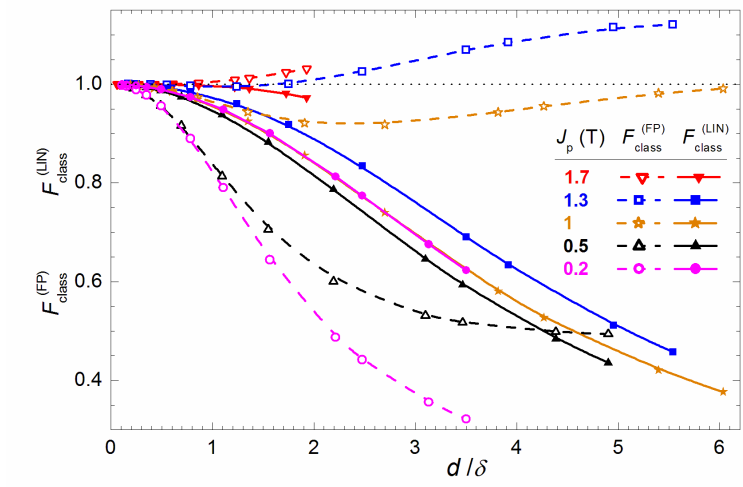


Fig. 7 - Ratios $F_{class}^{(FP)} = W_{class}^{(ROT,FP)}/W_{class}^{(ROT)}$ and $F_{class}^{(LIN)} = W_{class}^{(ROT,LIN)}/W_{class}^{(ROT)}$ (with $W_{class}^{(ROT)}$ given by Eq. (1)) calculated by the numerical method with Fixed Point iteration and the linear method. d/δ is the ratio between the sheet thickness and the skin depth.